

Correlation-driven Lifshitz transition and orbital order in a two-band Hubbard model

F. Grandi,¹ A. Amaricci,^{1,2} M. Capone,¹ and M. Fabrizio¹

¹*Scuola Internazionale Superiore di Studi Avanzati (SISSA), Via Bonomea 265, I-34136 Trieste, Italy*

²*CNR-IOM DEMOCRITOS, Istituto Officina dei Materiali,*

Consiglio Nazionale delle Ricerche, Via Bonomea 265, I-34136 Trieste, Italy

(Dated: September 6, 2018)

We study by dynamical mean field theory the ground state of a quarter-filled Hubbard model of two bands with different bandwidths. At half-filling, this model is known to display an orbital selective Mott transition, with the narrower band undergoing Mott localisation while the wider one being still itinerant. At quarter-filling, the physical behaviour is different and to some extent reversed. The interaction generates an effective crystal field splitting, absent in the Hamiltonian, that tends to empty the narrower band in favour of the wider one, which also become more correlated than the former at odds with the orbital selective paradigm. Upon increasing the interaction, the depletion of the narrower band can continue till it empties completely and the system undergoes a topological Lifshitz transition into a half-filled single-band metal that eventually turns insulating. Alternatively, when the two bandwidths are not too different, a first order Mott transition intervenes before the Lifshitz's one. The properties of the Mott insulator are significantly affected by the interplay between spin and orbital degrees of freedom.

I. INTRODUCTION

Orbital degrees of freedom in correlated materials have witnessed a revived interest in recent years mainly motivated by the physics of ruthenates^{1,2}, of iridates and other transition metal compounds with strong spin-orbit coupling^{3,4}, and of iron pnictides⁵⁻⁷. Realistic lattice Hamiltonians are characterised by tight-binding parameters generically not invariant under orbital $O(3)$ rotations. However, the sensitivity to such orbital symmetry breaking terms depends significantly on the degree of correlations, quantified by the strengths both of the monopole Slater integral, i.e. the conventional Hubbard U , as well as of the higher order multipoles responsible of Hund's rules. For instance, the distinction between different orbitals brought about by the hopping integrals and the crystal field can be amplified by strong correlations, leading to pronounced orbital differentiation⁷⁻¹⁰, and eventually to the so-called orbital-selective Mott transitions (OSMT)¹¹⁻²⁶ where the orbitals with the narrowest bandwidth localise while the others are still itinerant. In addition, orbital degrees of freedom are expected to play an important role in determining which symmetry-broken phase is more likely to accompany the Mott transition when correlations grow at integer electron density. This issue has been studied quite intensively deep inside the Mott insulator, where one can map the Hamiltonian onto a Kugel-Khomskii type²⁷⁻³⁰ of spin-orbital Heisenberg model³, while it is to a large extent unexplored right at the Mott transition.

In this work we tackle this issue and analyse how orbital degrees of freedom affect the zero temperature Mott transition in the simple two-band Hamiltonian where OSMT was first observed¹¹, though at quarter³¹ rather than at half-filling³²⁻³⁴. We will show that, despite its simplicity, this model acquires quite a rich phase diagram thanks to the orbital degrees of freedom and their interplay with the spin ones. The article is organised as

follows. In section II we introduce the model and anticipate its possible phases by simple weak and strong coupling arguments. In sections III and IV we present the solution of the model on a Bethe lattice with infinite coordination number through the dynamical mean-field theory. In particular, in section III we discuss the results obtained by preventing magnetic long-range order, which we instead allow in section IV. Finally, section V is devoted to concluding remarks.

II. THE MODEL

We consider the Hubbard model of two orbitals with different hopping integrals

$$\mathcal{H} = -\frac{1}{\sqrt{z}} \sum_{(\mathbf{R}\mathbf{R}'), \sigma} \sum_{a=1}^2 t_a \left(c_{\mathbf{R}a\sigma}^\dagger c_{\mathbf{R}'a\sigma} + H.c. \right) + \frac{U}{2} \sum_{\mathbf{R}} n_{\mathbf{R}} (n_{\mathbf{R}} - 1) - \mu \sum_{\mathbf{R}} n_{\mathbf{R}}, \quad (1)$$

on a Bethe lattice of coordination number z that we shall eventually send to infinity. In (1) the operator $c_{\mathbf{R}a\sigma}$ ($c_{\mathbf{R}a\sigma}^\dagger$) annihilates (creates) an electron at site \mathbf{R} in orbital $a = 1, 2$ with spin $\sigma = \uparrow, \downarrow$, $n_{\mathbf{R}} = \sum_{a\sigma} n_{\mathbf{R}a\sigma} = \sum_{a\sigma} c_{\mathbf{R}a\sigma}^\dagger c_{\mathbf{R}a\sigma}$ is the number operator at site \mathbf{R} , μ the chemical potential, and t_a a nearest neighbour hopping integral, diagonal in the orbital index a . Hereafter we shall assume $t_1 \geq t_2$ and define the hopping anisotropy parameter $\alpha = t_2/t_1 \in [0, 1]$.

At half-filling, i.e. an average occupation of two electrons per site, $\langle n_{\mathbf{R}} \rangle = 2$, the Hamiltonian (1) was first studied as the simplest toy model to uncover the physics of OSMT¹¹⁻¹³. The interaction U makes the narrower band more correlated than the wider one, as one would naïvely expect, to such an extent that band 2 may become Mott localised despite band 1 is still itinerant. This

phenomenon is paradigmatic of many physical situations, the best known examples being heavy fermions³⁵ and ruthenates¹.

Here we shall instead focus on the quarter-filled density case, i.e. $\langle n_{\mathbf{R}} \rangle = 1$. We consider an interaction term (see (1)) which includes the monopole Slater integral $U > 0$, but not the Coulomb exchange J responsible of Hund's rule. This term corresponds to the density-density part of the Kanamori interaction^{6,36} with no Hund's coupling.

We introduce the local spin and orbital pseudo-spin operators, $\boldsymbol{\sigma}_{\mathbf{R}}$ and $\boldsymbol{\tau}_{\mathbf{R}}$, respectively, through:

$$\begin{aligned}\boldsymbol{\sigma}_{\mathbf{R}} &= \sum_{a\sigma\sigma'} c_{\mathbf{R}a\sigma}^\dagger \boldsymbol{\sigma}_{\sigma\sigma'} c_{\mathbf{R}a\sigma'} , \\ \boldsymbol{\tau}_{\mathbf{R}} &= \sum_{\sigma ab} c_{\mathbf{R}a\sigma}^\dagger \boldsymbol{\sigma}_{ab} c_{\mathbf{R}b\sigma} ,\end{aligned}$$

where $\boldsymbol{\sigma} = (\sigma^x, \sigma^y, \sigma^z)$, with $\sigma^{x,y,z}$ being the Pauli matrices. The Hamiltonian (1) is invariant under global spin- $SU(2)$ rotations. On the contrary, orbital $SU(2)$ symmetry holds only at $\alpha = 1$, while for any $\alpha < 1$ the symmetry is lowered down to $U(1)$, which corresponds to uniform rotations around the orbital pseudo-spin z -axis. It follows that a finite expectation value of the z -component of the uniform pseudo-spin operator, which defines the orbital polarisation

$$\tau^z = \frac{1}{V} \sum_{\mathbf{R}\sigma} \langle n_{\mathbf{R}1\sigma} - n_{\mathbf{R}2\sigma} \rangle, \quad (2)$$

V being the number of lattice sites, is allowed by symmetry, while a finite expectation value of $\boldsymbol{\sigma}_{\mathbf{R}}$ and of $\boldsymbol{\tau}_{\mathbf{R}}^{x,y}$ would break a Hamiltonian symmetry, the spin $SU(2)$ and the orbital $U(1)$, respectively. We underline that when $\alpha = 1$ the symmetry of the model is enlarged to $SU(4)$ ³⁷, but in what follows we shall not consider such special point.

A. DMFT solution

We study the model Hamiltonian (1) by means of dynamical mean-field theory (DMFT). This is a non-perturbative method that provides an exact solution in the limit of infinite lattice-coordination $z \rightarrow \infty$.^{38,39} The non-interacting density-of-states corresponding to nearest-neighbour hopping t_a/\sqrt{z} , $a = 1, 2$, reads

$$D_a(\epsilon) = \frac{2}{\pi D_a^2} \sqrt{D_a^2 - \epsilon^2}, \quad (3)$$

where $D_a = 2t_a$ is half the bandwidth. Hereafter, we shall take $D_1 = 1$ as energy unit, so that $D_2 = \alpha \leq 1$. We observe that, since the Bethe lattice is bipartite and the Hamiltonian is not frustrated, the most likely spatial modulation breaks the symmetry between the two sub-lattices, which we shall label as sublattice $\Lambda = A$ and $\Lambda = B$. Within DMFT, the lattice model is mapped onto two distinct effective impurity problems, one for each

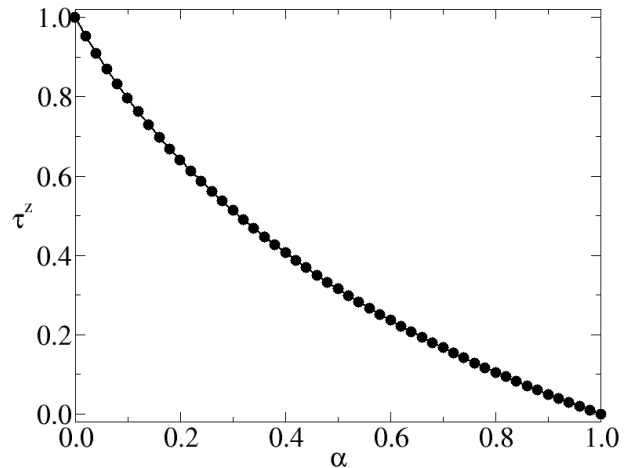


Figure 1. (Color online) Orbital polarization τ^z as function of α for the non interacting ($U = 0$) case.

sub-lattice. Each impurity is coupled to a self-consistent bath, which is described by a frequency dependent matrix Weiss field $\hat{G}_{0\Lambda}^{-1}(i\omega_n)$, whose matrix elements refer to spin and orbital indices. Each Weiss field is determined self-consistently by requiring the impurity problems to reproduce the local physics of the lattice model, which corresponds to the self-consistency equation:

$$\hat{G}_0^{-1}(i\omega_n) = \hat{G}_{\text{loc}}^{-1}(i\omega_n) + \hat{\Sigma}(i\omega_n) \quad (4)$$

where \hat{G}_{loc} is the local interacting Green's function of the lattice model, and $\hat{\Sigma}(i\omega_n)$ the impurity self-energy matrix. In this work we shall employ zero-temperature exact diagonalization as impurity solver^{40,41}, with a total number $N_s = 10$ of sites. This corresponds to a discretization of the bath of the effective Anderson model in $N_b = 8$ levels.⁴²

B. Weak and strong coupling analyses

We can actually anticipate some features of the phase diagram by simple arguments in the weak and strong coupling regimes, respectively.

1. Weak coupling

When $U = 0$, the system describes a quarter-filled two-band metal (2BM) with uniform orbital polarisation $\tau^z = 0$ at $\alpha = 1$ that increases monotonically as α decreases (see Fig. 1). A finite $U \ll \alpha$, small enough to justify the Hartree-Fock approximation, introduces an effective

crystal field splitting between the two bands

$$\begin{aligned} \mathcal{H} \rightarrow \mathcal{H}_{\text{HF}} = & -\frac{1}{\sqrt{z}} \sum_{\langle \mathbf{R}\mathbf{R}' \rangle, \sigma} \sum_{a=1}^2 t_a \left(c_{\mathbf{R}a\sigma}^\dagger c_{\mathbf{R}'a\sigma} + H.c. \right) \\ & - \sum_{\mathbf{R}} \left(\mu_{\text{HF}} n_{\mathbf{R}} + \Delta_{\mathbf{R}}^{\text{eff}} (n_{1\mathbf{R}} - n_{2\mathbf{R}}) \right), \end{aligned} \quad (5)$$

where^{43,44}

$$\Delta_{\mathbf{R}}^{\text{eff}} = \frac{U}{2} \langle n_{1\mathbf{R}} - n_{2\mathbf{R}} \rangle = \frac{U}{2} \tau^z, \quad \forall \mathbf{R}, \quad (6)$$

which, for any $\alpha < 1$, favours the occupation of the band 1 that has larger bandwidth. If such mean-field result remained valid even at sizeable U , we would expect a topological Lifshitz transition from a quarter-filled 2BM into a half-filled one-band metal (1BM). We note that, as long as the model remains in a quarter-filled 2BM phase, it is stable towards a Stoner-like instability with modulated magnetic and/or orbital ordering, which, in the present case, is expected to correspond to a translational symmetry breaking where the two-sublattice become inequivalent. On the contrary, the half-filled 1BM phase should become immediately unstable towards such symmetry breaking⁴⁵, turning the metal phase into an insulating one with magnetic and/or orbital ordering. In particular, since the hopping is diagonal in the orbital index, we expect a magnetic order that corresponds to a simple Néel antiferromagnet, where, because of spin $SU(2)$ invariance, symmetry can be broken along any spin direction. Conversely, the Hamiltonian for any $\alpha < 1$ is only invariant under orbital $U(1)$ rotations around the pseudo-spin z -axis. Therefore, the possible orbital orderings cannot be anticipated as simply as for the spin ones, and we must resort to some more sophisticated calculation. However, since all transitions are expected to occur at finite U , there is no guarantee that the above mean-field arguments hold, and thus the need of DMFT that is able to provide accurate results for any interaction strength.

2. Strong coupling

In order to foresee which orbital ordering is most likely to occur, we can still perform some simple analysis. Deep in the Mott insulator, i.e. at strong coupling $U \gg 1$, we can map the lattice model Eq. (1) onto an effective Kugel-Khomskii spin-orbital Heisenberg Hamil-

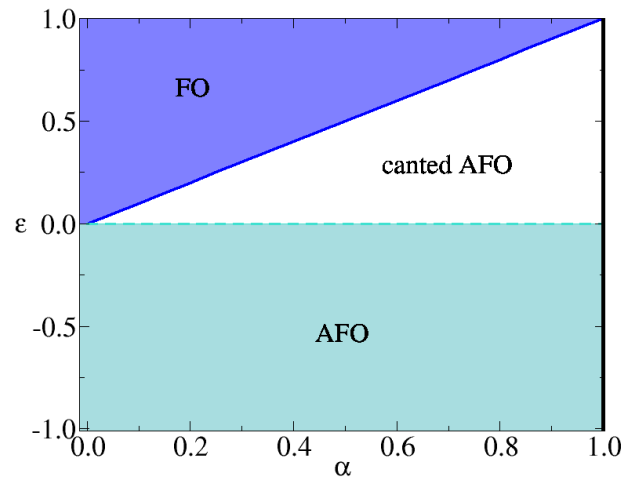


Figure 2. (Color online) Mean field phase diagram of the strong coupling Hamiltonian Eq. (7) as a function of α and of the phenomenological parameter ε , defined in Eq. (8). The diagram shows three distinct phases: a ferro- (FO) and an antiferro- (AFO) orbital state along the z -direction of the pseudospin and a canted AFO. The AFO phase is connected to the canted AFO through a first order transition (dashed line). The FO phase is separated from the canted AFO by a continuous transition (solid line). When $\varepsilon > 0$ ($\varepsilon < 0$) the system has antiferromagnetic (ferromagnetic) correlations. Along the line $\alpha = 1$ the model is $SU(4)$ invariant, and our simple mean field approximation does not apply any more.

tonian $\mathcal{H} \xrightarrow{U \gg 1} \mathcal{H}_{\text{KK}}$ ^{27,46}, where

$$\begin{aligned} \mathcal{H}_{\text{KK}} = & \frac{1}{z} \sum_{\langle \mathbf{R}\mathbf{R}' \rangle} \left\{ \frac{1}{16U} (1 + \boldsymbol{\sigma}_{\mathbf{R}} \cdot \boldsymbol{\sigma}_{\mathbf{R}'}) \left[(1 + \alpha^2) \right. \right. \\ & + (1 - \alpha^2) (\tau_{\mathbf{R}}^z + \tau_{\mathbf{R}'}^z) + (1 + \alpha^2) \tau_{\mathbf{R}}^z \tau_{\mathbf{R}'}^z \\ & \left. \left. + 2\alpha (\tau_{\mathbf{R}}^x \tau_{\mathbf{R}'}^x + \tau_{\mathbf{R}}^y \tau_{\mathbf{R}'}^y) \right] \right. \\ & \left. - \frac{1}{8U} (1 - \alpha^2) (\tau_{\mathbf{R}}^z + \tau_{\mathbf{R}'}^z) - \frac{1}{4U} (1 + \alpha^2) \right\}. \end{aligned} \quad (7)$$

We can solve this hamiltonian at the mean field level factorising the wavefunction into a spin part, $|\psi_{\sigma}\rangle$, and an orbital pseudo spin one, $|\psi_{\tau}\rangle$. We assume that the expectation value on the spin wavefunction

$$\langle \psi_{\sigma} | \boldsymbol{\sigma}_{\mathbf{R}} \cdot \boldsymbol{\sigma}_{\mathbf{R}'} | \psi_{\sigma} \rangle = -\varepsilon \in [-1, 1]. \quad (8)$$

Let us briefly comment about the meaning of Eq. (8). In a generic lattice

$$\langle \boldsymbol{\sigma}_{\mathbf{R}} \cdot \boldsymbol{\sigma}_{\mathbf{R}'} \rangle = \langle \boldsymbol{\sigma}_{\mathbf{R}} \rangle \cdot \langle \boldsymbol{\sigma}_{\mathbf{R}'} \rangle + \mathcal{O}\left(\frac{1}{z}\right), \quad (9)$$

so that in the limit of infinite coordination, $z \rightarrow \infty$, the parameter ε in Eq. (8) is finite as long as spin $SU(2)$

symmetry is broken, in which case the mean-field approximation predicts an antiferromagnetic spin configuration, $\varepsilon = 1$, and a ferro-orbital (FO) one, with expectation value $\langle \psi_\tau | \tau_{\mathbf{R}}^z | \psi_\tau \rangle = 1, \forall \mathbf{R}$. On the contrary, if we were to discuss the mean-field phase diagram of the Hamiltonian (7) in the paramagnetic sector and in the limit $z \rightarrow \infty$, we should, strictly speaking, set $\varepsilon = 0$. In this case the mean-field approximation for any $0 < \alpha < 1$ predicts two degenerate pseudo spin configurations, one, which we denote as antiferro-orbital (AFO), characterised by the finite expectation value $\langle \psi_\tau | \tau_{\mathbf{R}}^z | \psi_\tau \rangle = (-1)^R$, and the other, which we denote as canted antiferro-orbital (canted AFO), see Fig. 3, with non-zero expectation values

$$\begin{aligned} \langle \psi_\tau | (\cos \phi \tau_{\mathbf{R}}^x + \sin \phi \tau_{\mathbf{R}}^y) | \psi_\tau \rangle &= (-1)^R \tau^\parallel, \\ \langle \psi_\tau | \tau_{\mathbf{R}}^z | \psi_\tau \rangle &= \tau^z, \end{aligned} \quad (10)$$

where $\tau^z = \cos \theta = (1 - \alpha)/(1 + \alpha)$, $\tau^\parallel = \sin \theta$ and ϕ is free, signalling breaking of the orbital $U(1)$ symmetry. This result does not agree with DMFT, see below, which suggests that higher order terms in $1/U$, not included in Eq. (7), split the above accidental degeneracy. As a matter of fact, the actual DMFT phase diagram can be still rationalised through the mean-field treatment of the simple Hamiltonian (7), proviso a finite ε is assumed even in the paramagnetic sector and despite $z \rightarrow \infty$.

For the above reason, we shall hereafter take ε as a free parameter, in terms of which the phase diagram as function of α is that shown in Fig. 2. Whenever $\varepsilon < 0$ (ferromagnetic correlations) and $\alpha < 1$ the system is in an AFO state. When instead $\varepsilon > 0$, as physically expected, we find either a FO state for $\alpha < \varepsilon$ or a canted AFO one otherwise. The transition between the two phases is continuous within mean-field. Finally, for $\varepsilon = 0$, as we mentioned, the canted AFO and the AFO are accidentally degenerate. The transition between them is first order.

III. PARAMAGNETIC DMFT RESULTS

We now turn to exact DMFT and start by analysing the model (1) searching for paramagnetic solutions. However, since the Hamiltonian is not orbital pseudo-spin invariant, we cannot avoid orbital ordering.

We first consider an intermediate value of the bandwidth ratio $\alpha = 0.5$ and we show how the weakly interacting 2BM is driven to a Mott insulating state by increasing the interaction strength U . Such phase-transition is revealed by the evolution of the quasiparticle residue

$$Z_a = \left(1 - \frac{\partial \text{Re} \Sigma_{aa}(\omega)}{\partial \omega} \right)_{|\omega=0}^{-1}, \quad (11)$$

which quantifies the degree of Mott's localization of quasi-particles, being $Z_a \rightarrow 1$ in the non-interacting limit and $Z_a \rightarrow 0$ at the Mott transition.

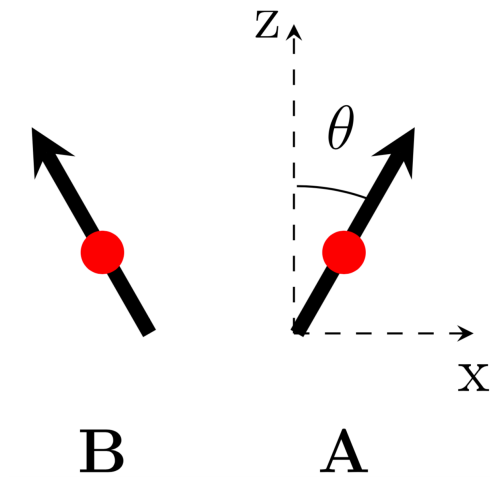


Figure 3. (Color online) Schematic representation of the canted AFO phase, assuming that the $U(1)$ symmetry is broken along x , i.e., $\phi = 0$ in Eq. (10). The arrows represent the configuration of the orbital pseudo-spin vectors τ at the two sites (red dots) A and B in the unit cell. θ is the angle between the z direction and the pseudospin τ on sublattice A (on sublattice B the angle has the value $-\theta$).

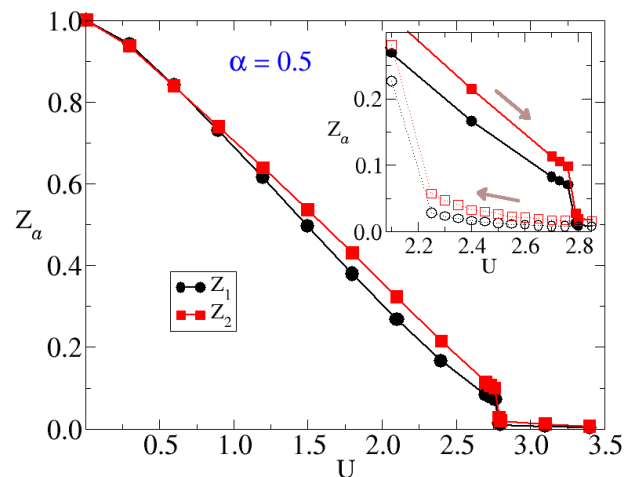


Figure 4. (Color online) The quasiparticle residues Z_a as function of U , for $\alpha = 0.5$. Both Z_1 and Z_2 vanish at $U = U_{c2} \simeq 2.80$ signalling transition to the Mott insulator. Inset: Hysteretic behavior of Z_a near the critical point. Filled (open) symbols are obtained continuing the solution from small (large) values of U .

The results for Z_a are reported in Fig. 4. In the weakly interacting regime the effects of the interaction are nearly identical on the two bands, i.e. $Z_1 \simeq Z_2$. However, upon increasing U , the two quantities start differentiating, with the wider band becoming more correlated than the narrower one, i.e. $Z_1 < Z_2$ ⁴⁷, at odds with the paradigm of the orbital selective Mott transition¹¹. At a critical value of U , the electrons on both bands localize, as signalled by the simultaneous vanishing of Z_1 and Z_2 . We find that the metal-insulator Mott transi-

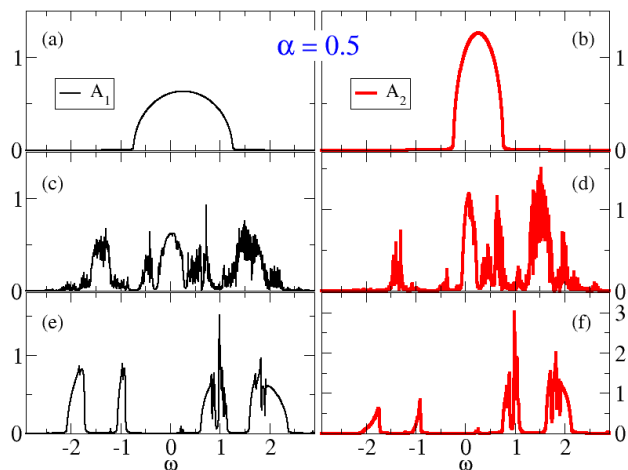


Figure 5. (Color online) The spectral functions $A_a(\omega)$ for $\alpha = 0.5$ and sublattice $\Lambda = A$. Data for $a = 1$ ($a = 2$) are reported on the left (right) column. The results are for increasing values of U : $U = 0.0$ (panels (a), (b)), $U = 2.1 < U_{c1}$ (panels (c), (d)), $U = 3.1 > U_{c2}$ (panels (e), (f)).

tion is first order. In the inset of Fig. 4 we show that Z_a at the transition suddenly jump to zero, and we also observe a clear hysteresis loop. The coexistence region extends between $U_{c1} \simeq 2.20$ and $U_{c2} \simeq 2.80$.

A direct insight into the solution is obtained by the evolution of the spectral functions $A_a(\omega) = -\frac{1}{\pi} \text{Im} G_{\text{loc}}^{aa}(\omega)$ with $a = 1, 2$, shown in Fig. 5. At $U = 0$ the spectral functions have the typical semi-elliptical shape of the Bethe lattice. Upon increasing the interaction, see Fig. 5(c)-(d), we observe at high-energy the gradual formation of the Hubbard sidebands, coexisting with the low-energy quasiparticle peaks. For $U > U_{c2}$ the system undergoes a transition into a Mott insulator. The corresponding spectral functions show a large gap around the Fermi level ($\omega = 0$) and the two Hubbard sidebands centred at about $\omega = \pm U/2$. We note that in the Mott insulator the band 2 has still weight below the Fermi level, namely, unlike the mean-field expectation, we do not find a transition into a one-band model with maximum orbital polarisation. In Fig. 6 we show the values of the uniform orbital polarization, τ^z , and staggered one, τ^{\parallel} , as function of U across the Mott transition. We always find a finite uniform polarisation, but also an antiferro-orbital polarisation in the xy -plane, which we have denoted as canted *AFO* state. This result suggests that the observed degeneracy between the *AFO* along the z direction and the canted *AFO* mentioned in Sec. II B 2 is removed in favor of the canted *AFO* state.

In the non-interacting limit, $\tau^{\parallel} = 0$ while the uniform orbital polarization along z is finite, due to the different bandwidths of the two orbitals. In agreement with mean-field, upon increasing U the wide band population grows at expenses of the narrow one, thus leading to an increase of τ^z while τ^{\parallel} remains zero. However this tendency does not proceed till a 2BM-to-1BM transition, i.e. till $\tau^z \rightarrow$

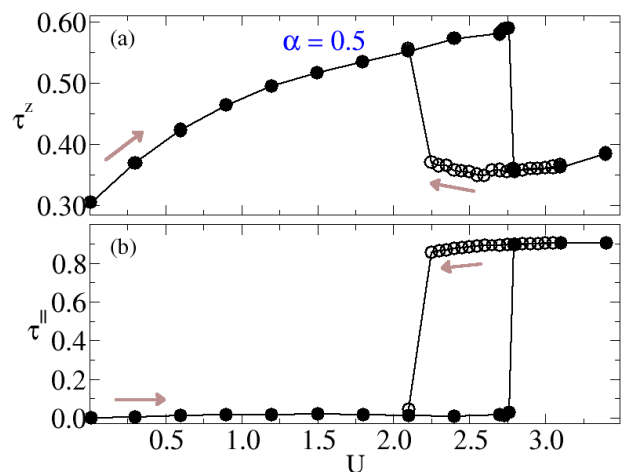


Figure 6. (Color online) Orbital polarization τ^z (a) and staggered in-plane component of the pseudospin τ^{\parallel} (b) as function of the interaction strength U . Data are for $\alpha = 0.5$. The arrow indicate the direction in the hysteresis cycle.

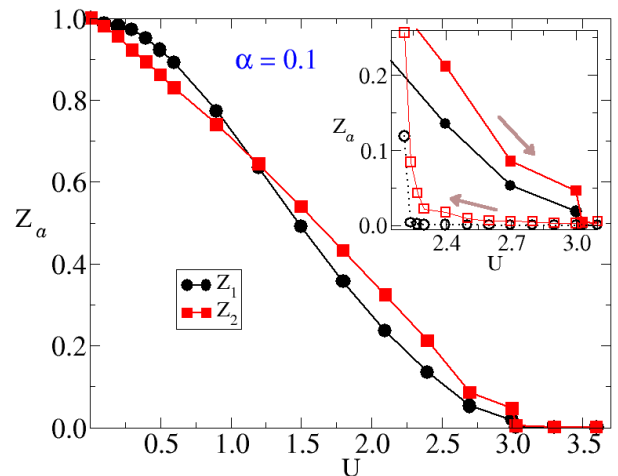


Figure 7. (Color online) Quasiparticle residues Z_a as function of U and for $\alpha = 0.1$. Inset: the same quantities near the first order transition. The arrows indicate the hysteresis cycle.

1; before that happens a first-order Mott transition takes place. At the transition, we find a sudden increase of τ^{\parallel} to an almost saturated value $\tau^{\parallel} \approx 0.9$, and, consequently, τ^z suddenly drops to a very small value, only slightly larger than the non-interacting one.

We now consider a smaller value of the bandwidth ratio, $\alpha = 0.1$. The large mismatch between the two bandwidth greatly enhances the occupation imbalance among the two orbitals, already in the uncorrelated regime. We start by the behaviour of the quasiparticle residues Z_a , shown in Fig. 7. Differently from the previous $\alpha = 0.5$ case, the two bands have distinct Z_a already at relatively small values of U , now with the narrower band more correlated than the wider one. This behaviour is reversed at $U \simeq 1.2$, at which the wider more populated band 1

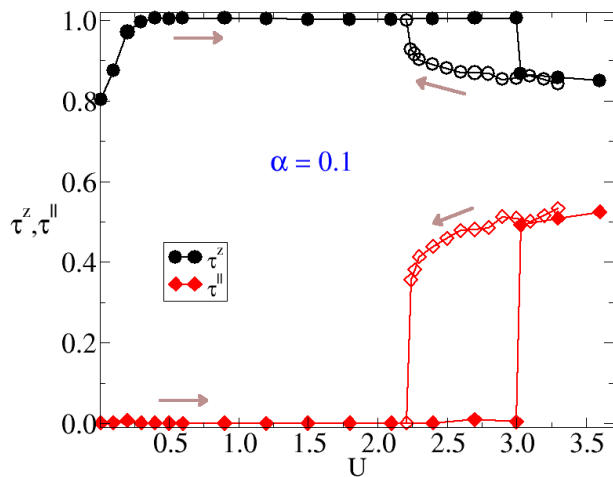


Figure 8. (Color online) Uniform orbital polarization, τ^z , and staggered one, τ^{\parallel} , as a function of U . Data are for $\alpha = 0.1$. The arrows indicate the hysteresis cycle near the Mott transition.

becomes also the most correlated one. Further increasing the correlation strength eventually drives the system into a Mott insulating state, as before through a first-order transition at which both quasiparticle residues drop to zero.

It is useful to compare the behaviour of Z_a with the evolution of the orbital polarisations τ^z and τ^{\parallel} , shown in Fig. 8. For very small U the system is characterised by a large value of uniform polarisation, τ^z , and vanishing staggered one, τ^{\parallel} . By slightly increasing the interaction strength, the orbital polarisation rapidly saturates to $\tau^z = 1$. Concomitantly, the narrower band empties while the wider one reaches half-filling. Therefore correlation drives in this case a continuous topological Lifshitz transition from a 2BM to a 1BM, as predicted by the Hartree-Fock approximation. Interestingly, the narrower band keeps a high degree of correlations, as demonstrated by the decreasing behaviour of Z_2 , see Fig. 7. In other words, although essentially empty, the band 2 is not completely decoupled from band 1.

More insights can be gained by the behaviour of the spectral functions, shown in Fig. 9. The large orbital occupation imbalance is already visible in the non-interacting limit, with the wider band being nearly centred around the Fermi level and, correspondingly, the narrower one nearly empty. Upon increasing the interaction U , the narrower band 2 gets shifted entirely above the Fermi level, yet it still shows spectral weight at high energy resulting from correlation effects. Simultaneously, the wider band recovers a particle-hole symmetric shape characterised by a three-peaks structure, with a renormalised central feature flanked by the two precursors of the Hubbard sidebands. For $U > U_{c2}$ a spectral gap opens in the half-filled wider band signalling the onset of a Mott insulating state. Notably, also the previously empty narrow band shows the formation of a Mott

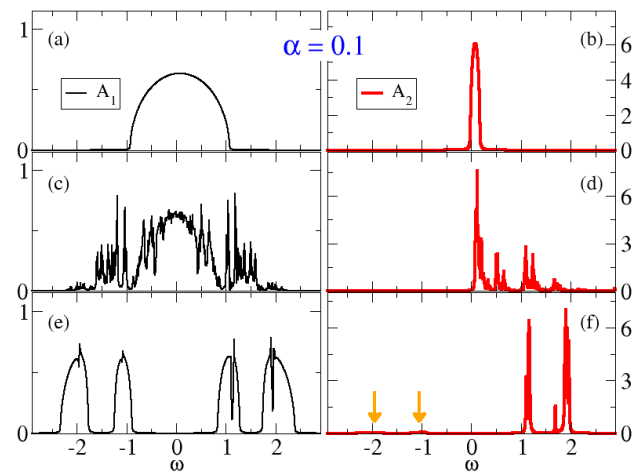


Figure 9. (Color online) Spectral functions for $\alpha = 0.1$ and fixed spin on sub-lattice A . Data are for increasing values of U : $U = 0.0$ ((a), (b)), $U = 1.2$ ((c), (d)) $U = 3.3$ ((e), (f)). Note the different scales in the y -axis. Arrows in panel (f) indicate tiny spectral weight below the Fermi level for narrow band.

gap which separates a large spectral feature above the Fermi level from a tiny spectral weight below it, see the arrows in Fig. 9(f). The system is thus characterized by $Z_1 = Z_2 = 0$ when it enters into the Mott state, see Fig. 7. As for the larger values of α , the resulting insulating state has a finite in-plane staggered polarization, τ^{\parallel} , and a reduced value of the uniform one, τ^z , see Fig. 8.

In order to ascertain the strong-coupling picture of section II B 2, we study the evolution of the orbital order in the Mott insulator at large U . In Fig. 10 we report the behaviour of both uniform, τ^z , and staggered, τ^{\parallel} , polarisations as function of α for $U = 5$. When $\alpha \rightarrow 0$, $\tau^z \rightarrow 1$ and $\tau^{\parallel} \rightarrow 0$, while the opposite occurs for $\alpha \rightarrow 1$. The evolution between these two limits is continuous, namely the critical $\alpha_c = 0$. We note that those results do not change by decreasing or increasing the interaction strength, provided the system remains within the insulating regime. This result further confirms the larger stability of the canted AFO with respect to the AFO along the z direction in the paramagnetic domain.

We summarise all previous results in the U - α phase diagram of Fig. 11. We find three distinct phases: a metallic state at small U and large enough α in which both bands are occupied (2BM); a metallic phase at small U and α with a half-filled wider band and an empty narrower one (1BM); a canted AFO ordered Mott insulator at large enough interaction. The two metallic phases are connected through a continuous Lifshitz transition⁴⁸ associated to the correlation induced emptying of the narrow band. For a generic value of α , increasing the interaction U drives the system into a Mott state through a first-order transition. This transition is associated with a large coexistence region (grey shaded area) for $U_{c1} < U < U_{c2}$ ⁴⁹. The merging of the Mott and the

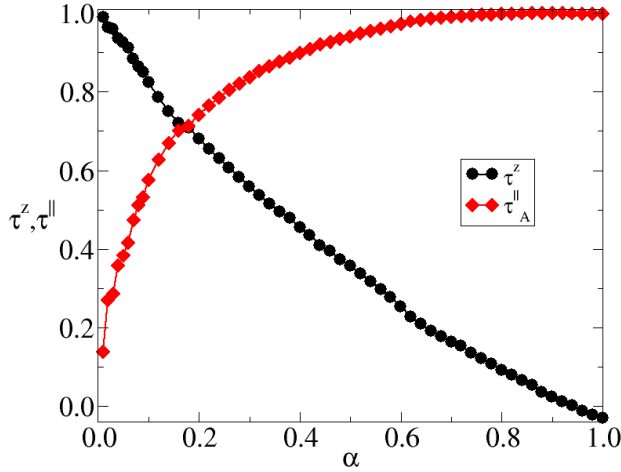


Figure 10. (Color online) Uniform orbital polarization τ^z and staggered in-plane component of the pseudospin τ^{\parallel} as function of α . Data are for $U = 5.0$.

Lifshitz transition line is a tricritical point⁵⁰. Interestingly, the insulator and the 1BM spinodal lines show a residual dependence on α . This reveals the strong entanglement between the two bands. Thus, although in the 1BM phase the wider band is half-filled and particle-hole symmetric, its description can not be simply reduced to that of a single-band Hubbard model. This description is recovered only in the limit $\alpha \rightarrow 0$, where just the broader band is filled for each value of the interaction strength. We emphasize that the quarter filling condition $\langle n_{\mathbf{R}} \rangle = 1$ differentiates this model from the Falicov-Kimball one⁵¹. We find that the 1BM to Mott insulator transition at $\alpha = 0$ takes place continuously at $U_c = U_{c2}$, as in the DMFT description of the Mott transition in the single-band Hubbard model³⁹. However, for any non-zero α a finite staggered in-plane polarisation appears, and thus both bands are partially occupied.

IV. ANTI-FERROMAGNETIC DMFT RESULTS

In the previous section we artificially prevented the DMFT solution to spontaneously break spin- $SU(2)$ symmetry and order magnetically, specifically into a simple Néel antiferromagnetic configuration since the lattice is bipartite and the Hamiltonian not frustrated. Here we shall instead leave the system free to order also magnetically, and study the interplay between spin and orbital orderings. Because of spin $SU(2)$ symmetry, all symmetry breaking directions are equivalent, and thus we choose for convenience the z -axis and define the staggered magnetisation of orbital $a = 1, 2$ as

$$m_a = \frac{1}{V} \sum_{\mathbf{R} \in A} \langle n_{\mathbf{R}a\uparrow} - n_{\mathbf{R}a\downarrow} \rangle - \frac{1}{V} \sum_{\mathbf{R} \in B} \langle n_{\mathbf{R}a\uparrow} - n_{\mathbf{R}a\downarrow} \rangle,$$

and the full staggered magnetisation as $m = m_1 + m_2$.

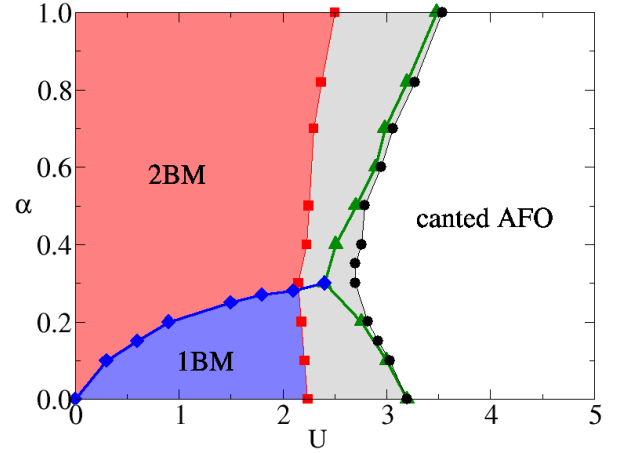


Figure 11. (Color online) The non-magnetic phase diagram of the model in the U - α plane. Three different phases are present: a two-bands metal (2BM) at small U and large enough α ; a one-band metal (1BM) for small α and small U ; and a Mott insulator with canted AFO order. The 2BM phase is connected to the 1BM through a continuous topological Lifshitz transition (diamonds). The transition to the canted AFO ordered Mott insulator is of first-order. The spinodal lines (filled circles and squares) delimitate the coexistence region. The first-order critical line (filled triangles) is computed from the energy crossing of the two solutions. A tricritical point is present at the merging of the transition line.

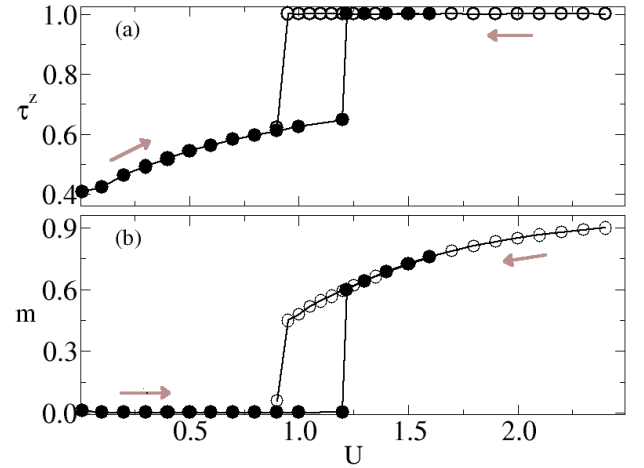


Figure 12. (Color online) Uniform orbital polarization τ^z (a) and staggered spin magnetization m (b) as functions of the interaction U . Data are for $\alpha = 0.4$. The system undergoes a first-order transition from the 2BM to an antiferromagnetic (AFM) state, with finite m . The orbital polarization saturates to $\tau^z = 1$ corresponding to a ferro-orbital (FO) ordering of the AFM state. The arrows indicate the directions of the solutions in the coexistence region $U_{c1}^{AFM} = 0.9 < U < 1.2 = U_{c2}^{AFM}$.

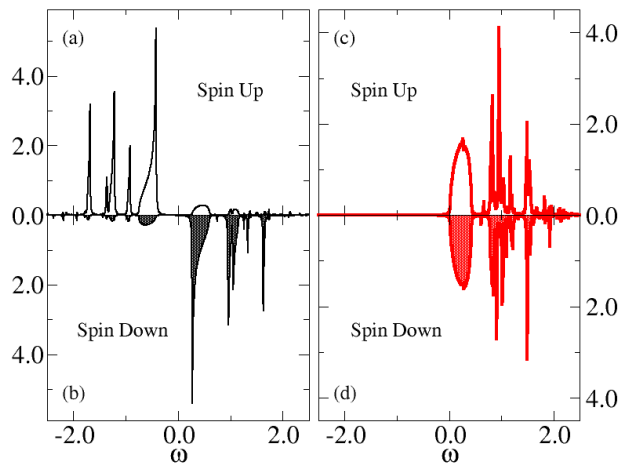


Figure 13. (Color online) Spin resolved spectral functions for $\alpha = 0.4$, sub-lattice $\Lambda = A$, corresponding to majority spin up, and $U = 1.6$. Data for the wide band are in panels (a)-(b), those for the narrow band in panels (c)-(d).

We start taking $\alpha = 0.4$. In Fig. 12 we show the evolution of the uniform orbital polarization τ^z and staggered magnetization m as function of U . By increasing the interaction from $U = 0$, τ^z slowly increases, but the system remains a paramagnetic 2BM, thus $m = 0$. For $U = U_{c2}^{AFM} \simeq 1.2$ we find a first-order transition to an antiferromagnetic (AFM) ordered state, signalled by the sudden increase of the staggered magnetization m . Concurrently, the uniform orbital polarization saturates, $\tau^z = 1$. We thus find that the magnetic transition appear simultaneously with the emptying of the narrow band, as expected by the Stoner instability of a half-filled single band.

We can gain insight into the nature of the AFM phase at large U by looking at the spin resolved spectral functions of the two orbitals, shown in Fig. 13. The wider band 1 has a particle-hole symmetric spectrum. Conversely, the narrower band lies entirely above the Fermi level.

We now study how the phase diagram changes with α . In Fig. 14 we show the dependence upon α of the staggered magnetisation and polarisation, m and τ^{\parallel} , respectively, and of the uniform orbital polarisation τ^z , deep in the insulating phase at $U = 4.5$. For $\alpha \lesssim 0.7$ we find the same behaviour as at $\alpha = 0.4$, $m \simeq 1$, $\tau^z \simeq 1$ and $\tau^{\parallel} = 0$. Surprisingly, at $\alpha \simeq 0.7$ we observe a second order transition, above which also the orbital $U(1)$ symmetry breaks spontaneously and the model develops a finite staggered polarisation τ^{\parallel} . The staggered magnetisation remains almost saturated, but now has contribution from both bands. Indeed, since for $\alpha < 1$ the solution corresponds to a canted AFO ordering, the system has a finite FO component along the z -direction of τ , ultimately giving rise to AFM correlations similar to the one-band case.

To get further insight in the nature of the AFM phase for $\alpha > 0.7$ we show in Fig. 15 the spin- and orbital-

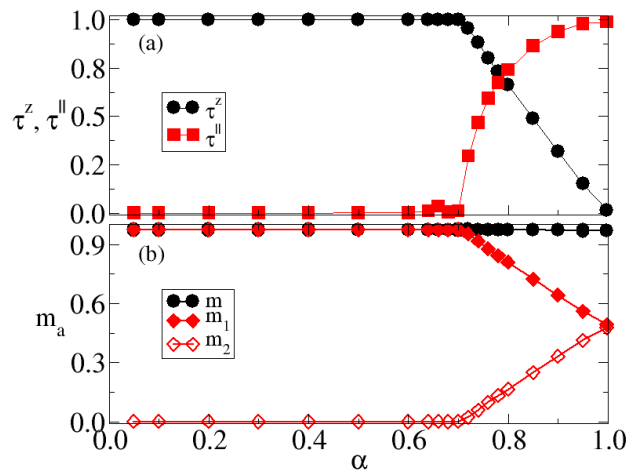


Figure 14. (Color online) (a) Uniform orbital polarization, τ^z , and staggered one, τ^{\parallel} , as function of α . (b) Total and orbital resolved staggered magnetization, m , m_1 and m_2 , as function of α . Data are for $U = 4.5$. The solution displays a continuous transition from the ferro-orbital antiferromagnetic state to a canted antiferro-orbital but still antiferromagnetic state at $\alpha \simeq 0.7$.

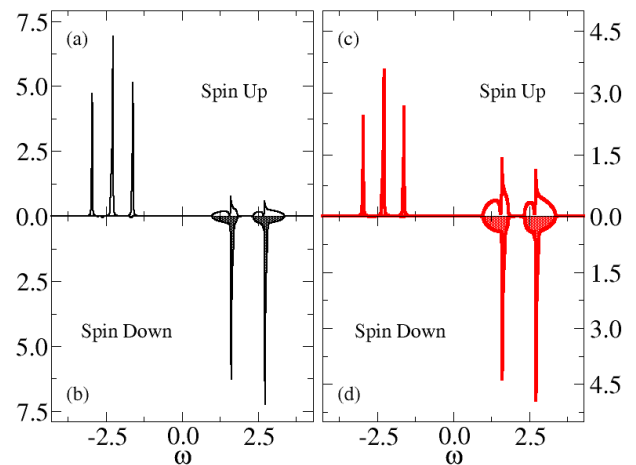


Figure 15. (Color online) Spin-resolved spectral functions for $\alpha = 0.9$ on sublattice A , $U = 4.5$ for the wide band ((a)-(b)) and the narrow one ((c)-(d)).

resolved spectral functions at $\alpha = 0.9$. It is instructive to compare these data with those reported in Fig. 13. For this larger value of the bandwidth ratio, the two orbitals have almost indistinguishable spectral functions, unlike below the transition at $\alpha \simeq 0.7$.

We summarise our findings in the magnetic phase diagram drawn in Fig. 16. We find three distinct phases. At small U the 2BM is stable. For larger U an AFM ordered insulator sets in. The magnetic transition is first-order, with a coexistence region that shrinks on approaching $\alpha = 0$. The magnetic transition takes place for any α and for values of U smaller than those required

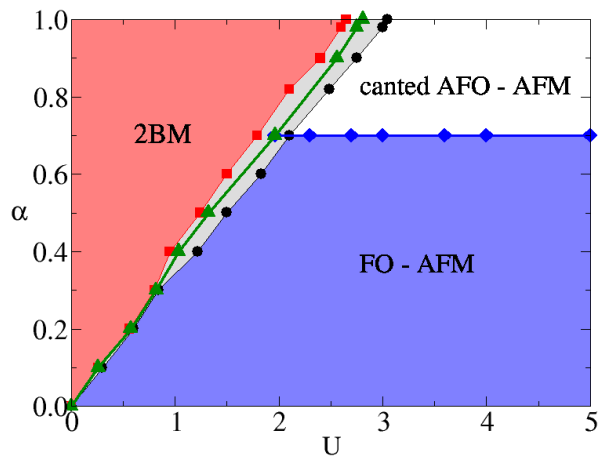


Figure 16. (Color online) Magnetic phase-diagram of the model in the U - α plane. The phase diagram shows two main regions: a paramagnetic 2BM for small values of the interaction U and an AFM insulator for $U > U_c^{AFM}$. The magnetic transition is of the first-order. The (gray) shaded area indicates the coexistence region. The AFM phase is further divided in two by a continuous transition: an AFM with a canted AFO order for $\alpha > 0.7$, and an AFM with full orbital polarisation for $\alpha < 0.7$.

in the absence of magnetism, i.e. $U_c^{AFM} < U_c$. In particular, as expected by comparison with the single-band Hubbard model, the 1BM region gets completely suppressed by the onset of AFM order. Moreover, the AFM phase is cut in two by a second order transition line associated with a change in orbital ordering. For $\alpha < 0.7$ the AFM has a saturated uniform orbital polarisation, in which only the wide band is occupied and contributes to the magnetic ordering. Increasing the bandwidth ratio above $\alpha \simeq 0.7$ leads to spontaneous orbital- $U(1)$ symmetry breaking, signalled by a finite in-plane staggered orbital polarisation. In this phase both bands are almost equally occupied and thus both contribute to the AFM order. Interestingly, we find that this transition is independent by the interaction strength U and that we can reproduce it at the mean field level by assuming a value $\varepsilon \approx 0.7$ for the spin-spin correlation parameter that appears in Fig. 2.

We emphasise that the above results are valid as long as $\alpha < 1$. When $\alpha = 1$ the enlarged $SU(4)$ symmetry of the model may entail different type of spin-orbital orders³⁷ that we did not analyse.

V. CONCLUSIONS

Despite its simplicity, two bands with different bandwidths subject to a monopole Slater integral U and at quarter-filling, the model (1) shows a remarkably rich phase diagram once the interplay between orbital and spin degrees of freedom are fully taken into account. In

particular, because of the bandwidth difference, the interaction U generates an effective crystal field that tends to empty the narrower band. This shows that correlations may not just enhance an existing crystal field, as pointed out in Ref. 52 in connection with the physics of V_2O_3 , but even generate one despite its absence in the original Hamiltonian. The depletion of the narrower band continues till a topological Lifshitz transition occurs, above which only the wider band remains occupied, and specifically half-filled. In our case study, with a bipartite lattice and unfrustrated Hamiltonian, as soon as the narrower band empties, a Stoner instability takes place driving the half-filled wider band into an antiferromagnetic insulator. This magnetic insulator still shows an active role of the orbital degrees of freedom that can drive a further phase transition between an insulator where only the wider band is occupied into another one where a canted antiferro-orbital order appears, and thus both bands are populated. The physics of the magnetic insulator observed at $\alpha \approx 1$ can describe some of the properties of the $KCuF_3$ compound^{53,54}. However, we would like to emphasize that in the present work does not take into account the strong directionality of the e_g bands in d -orbitals compounds, which makes the comparison with realistic materials hard. Such important effect is left for future work in this direction.

We argue that, in a generic situation where some degree of frustration is unavoidably present, either geometric or caused by longer range hopping integrals, the one-band metal, with only the wider band occupied, might remain stable till a finite U Mott transition, as we indeed found by preventing magnetism. We thus expect that the generic phase diagram must include, for not too strong repulsion U , a quarter-filled two-band metal separated by an interaction-induced Lifshitz transition from a half-filled one-band metal. Both metal phases must eventually give way to a Mott insulator above a critical U , whose precise magnetic and orbital properties will critically depend on the degree of frustration. We end emphasising that, at odds with the naïve expectation that a narrower band must also be the more correlated one, we here find right the opposite. This effect is due to the effective crystal field Δ^{eff} that progressively empties the narrow band and at the same time brings the broad band closer and closer to the half filling condition, enhancing the correlation effect on the wider band.

ACKNOWLEDGEMENTS

We acknowledge support from the H2020 Framework Programme, under ERC Advanced Grant No. 692670 “FIRSTORM”. A.A. and M.C. also acknowledge financial support from MIUR PRIN 2015 (Prot. 2015C5SEJJ001) and SISSA/CNR project “Superconductivity, Ferroelectricity and Magnetism in bad metals” (Prot. 232/2015).

- ¹ V.I. Anisimov, I.A. Nekrasov, D.E. Kondakov, T.M. Rice, and M. Sigris, “Orbital-selective Mott-insulator transition in $\text{Ca}_{2-x}\text{Sr}_x\text{RuO}_4$,” *The European Physical Journal B - Condensed Matter and Complex Systems* **25**, 191–201 (2002).
- ² S. Nakatsuji and Y. Maeno, “Quasi-two-dimensional mott transition system $\text{Ca}_{2-x}\text{Sr}_x\text{RuO}_4$,” *Phys. Rev. Lett.* **84**, 2666–2669 (2000).
- ³ G. Jackeli and G. Khaliullin, “Mott insulators in the strong spin-orbit coupling limit: From heisenberg to a quantum compass and kitaev models,” *Phys. Rev. Lett.* **102**, 017205 (2009).
- ⁴ Jeffrey G. Rau, Eric Kin-Ho Lee, and Hae-Young Kee, “Spin-orbit physics giving rise to novel phases in correlated systems: Iridates and related materials,” *Annual Review of Condensed Matter Physics* **7**, 195–221 (2016), <https://doi.org/10.1146/annurev-conmatphys-031115-011319>.
- ⁵ Luca de’ Medici, Jernej Mravlje, and Antoine Georges, “Janus-Faced Influence of Hund’s Rule Coupling in Strongly Correlated Materials,” *Phys. Rev. Lett.* **107**, 256401 (2011).
- ⁶ Antoine Georges, Luca de’ Medici, and Jernej Mravlje, “Strong correlations from hund’s coupling,” *Annual Review of Condensed Matter Physics* **4**, 137–178 (2013).
- ⁷ Luca de’ Medici, Gianluca Giovannetti, and Massimo Capone, “Selective Mott physics as a key to iron superconductors,” *Phys. Rev. Lett.* **112**, 177001 (2014).
- ⁸ Z. P. Yin, K. Haule, and G. Kotliar, “Kinetic frustration and the nature of the magnetic and paramagnetic states in iron pnictides and iron chalcogenides,” *Nature Materials* **10**, 932 EP – (2011).
- ⁹ E. Bascones, B. Valenzuela, and M. J. Calderón, “Orbital differentiation and the role of orbital ordering in the magnetic state of fe superconductors,” *Phys. Rev. B* **86**, 174508 (2012).
- ¹⁰ Nicola Lanatà, Yongxin Yao, Xiaoyu Deng, Vladimir Dobrosavljević, and Gabriel Kotliar, “Slave boson theory of orbital differentiation with crystal field effects: Application to UO_2 ,” *Phys. Rev. Lett.* **118**, 126401 (2017).
- ¹¹ Akihisa Koga, Norio Kawakami, T. M. Rice, and Manfred Sigris, “Orbital-selective mott transitions in the degenerate hubbard model,” *Phys. Rev. Lett.* **92**, 216402 (2004).
- ¹² Michel Ferrero, Federico Becca, Michele Fabrizio, and Massimo Capone, “Dynamical behavior across the mott transition of two bands with different bandwidths,” *Phys. Rev. B* **72**, 205126 (2005).
- ¹³ Luca de’ Medici, Antoine Georges, and Silke Biermann, “Orbital-selective Mott transition in multiband systems: Slave-spin representation and dynamical mean-field theory,” *Phys. Rev. B* **72**, 205124 (2005).
- ¹⁴ Eberhard Jakobi, Nils Blümer, and Peter van Dongen, “Orbital-selective mott transitions in a doped two-band hubbard model with crystal field splitting,” *Phys. Rev. B* **87**, 205135 (2013).
- ¹⁵ E. A. Winograd and L. de’ Medici, “Hybridizing localized and itinerant electrons: A recipe for pseudogaps,” *Phys. Rev. B* **89**, 085127 (2014).
- ¹⁶ Luca de’ Medici, “Hund’s coupling and its key role in tuning multiorbital correlations,” *Phys. Rev. B* **83**, 205112 (2011).
- ¹⁷ Tomoko Kita, Takuma Ohashi, and Norio Kawakami, “Mott transition in three-orbital hubbard model with orbital splitting,” *Phys. Rev. B* **84**, 195130 (2011).
- ¹⁸ Yilin Wang, Li Huang, Liang Du, and Xi Dai, “Doping-driven orbital-selective mott transition in multi-band hubbard models with crystal field splitting,” *Chinese Physics B* **25**, 037103 (2016).
- ¹⁹ Luca de’ Medici, S. R. Hassan, Massimo Capone, and Xi Dai, “Orbital-selective mott transition out of band degeneracy lifting,” *Phys. Rev. Lett.* **102**, 126401 (2009).
- ²⁰ Yashar Komijani and Gabriel Kotliar, “Analytical slave-spin mean-field approach to orbital selective mott insulators,” *Phys. Rev. B* **96**, 125111 (2017).
- ²¹ Rong Yu and Qimiao Si, “Orbital-selective mott phase in multiorbital models for iron pnictides and chalcogenides,” *Phys. Rev. B* **96**, 125110 (2017).
- ²² Shintaro Hoshino and Philipp Werner, “Spontaneous orbital-selective mott transitions and the jahn-teller metal of A_3C_{60} ,” *Phys. Rev. Lett.* **118**, 177002 (2017).
- ²³ Li Huang, Yilin Wang, Lei Wang, and Philipp Werner, “Detecting phase transitions and crossovers in hubbard models using the fidelity susceptibility,” *Phys. Rev. B* **94**, 235110 (2016).
- ²⁴ Philipp Werner, Emanuel Gull, and Andrew J. Millis, “Metal-insulator phase diagram and orbital selectivity in three-orbital models with rotationally invariant hund coupling,” *Phys. Rev. B* **79**, 115119 (2009).
- ²⁵ K. Bouadim, G. G. Batrouni, and R. T. Scalettar, “Determinant quantum monte carlo study of the orbitally selective mott transition,” *Phys. Rev. Lett.* **102**, 226402 (2009).
- ²⁶ Luca F Tocchio, Federico Arrigoni, Sandro Sorella, and Federico Becca, “Assessing the orbital selective mott transition with variational wave functions,” *Journal of Physics: Condensed Matter* **28**, 105602 (2016).
- ²⁷ K. I. Kugel and D. I. Khomskii, “Crystal-structure and magnetic properties of substances with orbital degeneracy,” *Zh. Eksp. Teor. Fiz* **64**, 1429–1439 (1973).
- ²⁸ Kliment I Kugel’ and D I Khomski, “The jahn-teller effect and magnetism: transition metal compounds,” *Soviet Physics Uspekhi* **25**, 231 (1982).
- ²⁹ L.-M. Duan, E. Demler, and M. D. Lukin, “Controlling spin exchange interactions of ultracold atoms in optical lattices,” *Phys. Rev. Lett.* **91**, 090402 (2003).
- ³⁰ D I Khomskii, “Role of orbitals in the physics of correlated electron systems,” *Physica Scripta* **72**, CC8 (2005).
- ³¹ Satoshi Miyashita, Yasufumi Yamashita, Kenji Yonemitsu, Akihisa Koga, and Norio Kawakami, “Mott insulating state in a quarter-filled two-orbital hubbard chain with different bandwidths,” *Journal of Physics: Conference Series* **150**, 042128 (2009).
- ³² Marcelo J. Rozenberg, “Integer-filling metal-insulator transitions in the degenerate hubbard model,” *Phys. Rev. B* **55**, R4855–R4858 (1997).
- ³³ Nicola Manini, Giuseppe E. Santoro, Andrea DalCorso, and Erio Tosatti, “Sensitivity of the mott transition to noncubic splitting of the orbital degeneracy: Application to $\text{nh}_3\text{k}_3\text{C}_{60}$,” *Phys. Rev. B* **66**, 115107 (2002).
- ³⁴ Robert Peters and Thomas Pruschke, “Orbital and magnetic order in the two-orbital hubbard model,” *Phys. Rev. B* **81**, 035112 (2010).

- ³⁵ Matthias Vojta, “Orbital-selective Mott transitions: Heavy fermions and beyond,” *Journal of Low Temperature Physics* **161**, 203–232 (2010).
- ³⁶ Junjiro Kanamori, “Electron correlation and ferromagnetism of transition metals,” *Progress of Theoretical Physics* **30**, 275–289 (1963).
- ³⁷ Philippe Corboz, Andreas M. Läuchli, Karlo Penc, Matthias Troyer, and Frédéric Mila, “Simultaneous dimerization and $su(4)$ symmetry breaking of 4-color fermions on the square lattice,” *Phys. Rev. Lett.* **107**, 215301 (2011).
- ³⁸ Walter Metzner and Dieter Vollhardt, “Correlated lattice fermions in $d = \infty$ dimensions,” *Phys. Rev. Lett.* **62**, 324–327 (1989).
- ³⁹ Antoine Georges, Gabriel Kotliar, Werner Krauth, and Marcelo J. Rozenberg, “Dynamical mean-field theory of strongly correlated fermion systems and the limit of infinite dimensions,” *Rev. Mod. Phys.* **68**, 13–125 (1996).
- ⁴⁰ Michel Caffarel and Werner Krauth, “Exact diagonalization approach to correlated fermions in infinite dimensions: Mott transition and superconductivity,” *Physical review letters* **72**, 1545–1548 (1994).
- ⁴¹ C. Weber, A. Amaricci, M. Capone, and P. B. Littlewood, “Augmented hybrid exact-diagonalization solver for dynamical mean field theory,” *Phys. Rev. B* **86**, 115136 (2012).
- ⁴² We performed calculations with different number of bath sites for selected points in the phase diagram in order to check the convergence of our results. We observed that qualitatively and quantitatively identical results are obtained already for $N_b = 8$. We stress that the bath parameters are determined self consistently in order to fulfill the DMFT self consistency equations, so they are adaptive. This reduces a lot the finite size effects on the solution of the problem, making this approach accurate already with relatively few bath levels.
- ⁴³ Matteo Sandri, Massimo Capone, and Michele Fabrizio, “Finite-temperature gutzwiller approximation and the phase diagram of a toy model for v_2O_3 ,” *Phys. Rev. B* **87**, 205108 (2013).
- ⁴⁴ Matteo Sandri and Michele Fabrizio, “Nonequilibrium gap collapse near a first-order mott transition,” *Phys. Rev. B* **91**, 115102 (2015).
- ⁴⁵ J. E. Hirsch, “Two-dimensional hubbard model: Numerical simulation study,” *Phys. Rev. B* **31**, 4403–4419 (1985).
- ⁴⁶ P. W. Anderson, “New approach to the theory of superexchange interactions,” *Phys. Rev.* **115**, 2–13 (1959).
- ⁴⁷ Tung-Lam Dao, Michel Ferrero, Pablo S. Cornaglia, and Massimo Capone, “Mott transition of fermionic mixtures with mass imbalance in optical lattices,” *Phys. Rev. A* **85**, 013606 (2012).
- ⁴⁸ I. M. Lifshitz, “Anomalies of electron characteristics of a metal in the high pressure region,” *Sov. Phys. JETP* **11**, 1130 (1960).
- ⁴⁹ K Binder, “Theory of first-order phase transitions,” *Reports on Progress in Physics* **50**, 783 (1987).
- ⁵⁰ Robert B. Griffiths, “Thermodynamics near the two-fluid critical mixing point in $he^3 - he^4$,” *Phys. Rev. Lett.* **24**, 715–717 (1970).
- ⁵¹ L. M. Falicov and J. C. Kimball, “Simple model for semiconductor-metal transitions: Smb_6 and transition-metal oxides,” *Phys. Rev. Lett.* **22**, 997–999 (1969).
- ⁵² Alexander I. Poteryaev, Jan M. Tomczak, Silke Biermann, Antoine Georges, Alexander I. Lichtenstein, Alexey N. Rubtsov, Tanusri Saha-Dasgupta, and Ole K. Andersen, “Enhanced crystal-field splitting and orbital-selective coherence induced by strong correlations in v_2O_3 ,” *Phys. Rev. B* **76**, 085127 (2007).
- ⁵³ L. Paolasini, R. Caciuffo, A. Sollier, P. Ghigna, and M. Altarelli, “Coupling between spin and orbital degrees of freedom in $kcuf_3$,” *Phys. Rev. Lett.* **88**, 106403 (2002).
- ⁵⁴ E. Pavarini, E. Koch, and A. I. Lichtenstein, “Mechanism for orbital ordering in $kcuf_3$,” *Phys. Rev. Lett.* **101**, 266405 (2008).